Interictal Spikes in Animal Models of Alzheimer's Disease: Dominance of the Dentate Gyrus and Cholinergic Control by Medial Septum

Christos Panagiotis Lisgaras[1, 2], Ph.D. and Helen E. Scharfman*[1, 2], Ph.D.

[1]Departments of Child & Adolescent Psychiatry, Neuroscience & Physiology, and Psychiatry, and the Neuroscience Institute
New York University Langone Health
550 First Ave.
New York, NY 10016

[2]Center for Dementia Research
The Nathan Kline Institute for Psychiatric Research
New York State Office of Mental Health
140 Old Orangeburg Road, Bldg. 35
Orangeburg, NY 10962

***Corresponding author:**
Helen E. Scharfman
The Nathan Kline Institute
Center for Dementia Research
140 Old Orangeburg Rd. Bldg. 35
Orangeburg, NY 10962

E-Mail: hscharfman@nki.rfmh.org
Alternates: helensch@optonline.net
christos.lisgaras@nyulangone.org
Phone: 845-398-5427
Fax: 845-398-5422

Running head: IIS in Animal Models of AD

Number of words whole text: 5339
Number of figures: 6
Number of tables: 0

Key words: Alzheimer's disease, APPSwe, Presenilin 2, Down's syndrome, cholinergic neurons, Interictal spikes, medial septum, septohippocampal

Abbreviations:
AD = Alzheimer's disease
DG = Dentate gyrus
IIS = Interictal spike
MS = Medial septum
PS2KO = Presenilin 2 knockout
REM = Rapid eye movement sleep
SWS = Slow-wave sleep

ABSTRACT

Interictal spikes (IIS) are a common type of abnormal electrical activity in animal models of Alzheimer's disease (AD) and AD patients. The brain regions where IIS are largest are not known but are important because such data would suggest sites that contribute to IIS generation. Because hippocampus and cortex exhibit altered excitability in AD models, we asked where IIS are largest along the cortical-CA1-dentate gyrus (DG) dorso-ventral axis. Because medial septal (MS) cholinergic neurons are overactive when IIS typically occur, we also tested the novel hypothesis that silencing the medial septohippocampal cholinergic neurons selectively would reduce IIS. We used 3 models of AD, Tg2576 mice, presenilin 2 knockout mice, and the Ts65Dn mouse model of Down's syndrome. To selectively silence MS cholinergic neurons, Tg2576 mice were bred with ChAT-Cre mice and offspring mice were injected in the MS with AAV encoding inhibitory designer receptors exclusively activated by designer drugs. We recorded EEG along the cortical-CA1-DG axis using silicon probes during wakefulness, slow-wave sleep (SWS) and rapid eye movement (REM) sleep.

We detected IIS in all transgenic mice but not age-matched controls. IIS were detectable throughout the cortical-CA1-DG axis and were primarily during REM sleep. In all 3 models, IIS amplitudes were significantly greater in the DG granule cell layer vs. CA1 pyramidal layer or overlying cortex. Selective chemogenetic silencing of MS cholinergic neurons significantly reduced IIS frequency during REM sleep without affecting the overall duration or number of REM sleep bouts.

Maximal IIS amplitude in the DG of 3 AD mouse models suggests that the DG could be one of the areas that contribute to IIS generation. Selectively reducing MS cholinergic tone could be a new strategy to reduce IIS in AD.

HIGHLIGHTS

- Interictal spikes (IIS) occurred in 3 Alzheimer's disease (AD) models and were most robust in REM sleep.
- In all 3 models, the DG granule cell layer exhibited a significantly greater IIS amplitude than all other recording sites.
- Selective chemogenetic silencing of medial septum cholinergic neurons significantly reduced IIS frequency during REM sleep.

INTRODUCTION

Abnormal electrical activity is gaining attention as an underappreciated contributor to Alzheimer's disease (AD) pathophysiology.[1-5] Abnormal electrical activity has been reported in humans with AD[6,7] and numerous animal models that simulate AD.[8-14] Although outright seizures in AD may be rare,[15] intermittent abnormal electrical activity is much more frequent than seizures,[16] and may occur at earlier disease stages than seizures.[11,14] Thus, targeting intermittent abnormal electrical activity in AD offers the opportunity to intervene early during AD progression when treatments are more likely to succeed.[17]

One of the earliest types of abnormal electrical activity in AD models are Interictal spikes (IIS)[1,11] and high frequency oscillations (HFOs).[14] IIS in epilepsy are known to impair cognition[18,19] and they are found to do so in AD as well.[16,20,21] Indeed, anti-seizure medications (ASMs) can improve cognition in those AD patients that show IIS in the EEG.[22] Also, IIS in AD models[8,10,11] and humans with AD[6,16] are known to occur during sleep which suggests that they may impair sleep-dependent memory consolidation.[23]

Despite the robust occurrence of IIS in AD, the exact origin of IIS in AD is currently unknown. One of the reasons for this gap in knowledge may be related to the silent nature of IIS and thus undetectability using conventional (non-invasive) EEG monitoring. In this context, minimally invasive approaches were instrumental in pointing to the temporal lobe as one of the areas where IIS and seizures can be robust.[6,24] A neuroimaging study in amnestic patients has provided even greater resolution on the possible sources of increased excitability within the hippocampus.[25] Indeed, the study[25] showed that within the hippocampus, area CA3 and the dentate gyrus (DG) were the hotspots of increased excitability. Nevertheless, detailed electrophysiological recordings of IIS in AD are limited because EEG monitoring is not common clinical practice. In this context, animal models are useful because the circuits involved in abnormal electrical activity could be examined in greater detail using invasive electrophysiological approaches.

We have shown that a new type of abnormal electrical activity in AD mouse models termed HFOs can be recorded primarily from the granule cell layer (GCL) of the DG.[14] Here we ask whether the DG is one of areas where IIS are most robust in amplitude compared to other regions such as area CA1 and overlying cortex. Thus, we analyzed IIS along the cortical-CA1-DG dorso-ventral axis. We recorded IIS in 3 AD mouse models each with a different causal mechanism. In all AD models, IIS were robust during rapid eye movement sleep (REM), a sleep stage when cholinergic tone is typically increased.[26,27] We also found that IIS showed an amplitude gradient along the cortical-CA1-DG axis with IIS amplitude significantly greater in the DG GCL compared to hippocampal area CA1 and the overlying cortical layers.

We next asked why IIS occur during sleep and specifically REM sleep. REM sleep is a sleep stage when cholinergic tone is significantly increased compared to non-REM (NREM) sleep.[26,27] In epilepsy, increased cholinergic tone is thought to facilitate epileptiform activity and seizures.[28,29] In an AD mouse model the cholinergic antagonist atropine reduced IIS in REM sleep, however this effect was confounded by a parallel reduction in REM sleep duration.[11] Thus, direct evidence for a possible contributing role of the cholinergic system on IIS generation is currently lacking.

Here we focused on selective targeting of the cholinergic neurons that give rise to the most dense projection to the hippocampus and are already implicated in memory[30,31] and AD pathophysiology,[32-35] the medial septum (MS) cholinergic neurons. Importantly, we found that the number of IIS during REM sleep was significantly reduced upon MS cholinergic silencing compared to the baseline number of IIS during REM sleep. It is notable that the reduction in the number of IIS during REM sleep was not due to reduced REM sleep duration, or reduced number of REM bouts compared to baseline REM sleep.

In summary, our data provide novel insight into IIS generation along the cortical-CA1-DG axis of 3 animal models of AD. We also provide new evidence for a contributing role of MS cholinergic

neurons in IIS. The mechanisms generating IIS and the cholinergic control of IIS in AD are important because they could lead to new therapeutic strategies.

MATERIALS AND METHODS

I. Animal care and models

We used 3 mouse models of AD each with a different AD causal mechanism and neuropathology. We refer to mice carrying a mutation (Tg2576$^{+/-}$, PS2KO$^{-/-}$, Ts65Dn) as transgenic and their wild type littermates (Tg2576$^{-/-}$, PS2KO$^{+/+}$, 2n, respectively) as controls. Tg2576 mice were bred on a C57BL6/SJL background (stock #100012, The Jackson Laboratory) and PS2KO and Ts65Dn mice on a C57BL/6J (stock #000664, The Jackson Laboratory) background. All mice were fed Purina 5001 (W.F. Fisher) with water *ad libitum*. Cages were filled with corn cob bedding and there was a 12 hr light:dark cycle (7:00 a.m. lights on, 7:00 p.m. lights off). Genotyping was performed by the Mouse Genotyping Core Laboratory at NYU Langone Medical Center or in-house. All experimental procedures were performed in accordance with the NIH guidelines and approved by the Institutional Animal Care and Use Committee at the Nathan Kline Institute.

Tg2576 transgenic mice overexpress the human amyloid precursor protein (APP) using the hamster prion promoter and have the Swedish mutation (APP_{Swe}) in APP isoform 695.[36] Tg2576 transgenic mice show memory deficits at the age of 3-4 months[37] and amyloid-β (Aβ) plaques by 6[11,38] and 12[36,38] months of age, respectively. Tg2576 transgenic mice were 5.5±2.4 months-old (range 1-19 months) at the time of EEG recording. Tg2576 control mice were 5.3±3.1 months-old (range 1-18 months). No statistically significant age differences were found between control and transgenic Tg2576 mice (Mann-Whitney *U*-test, U=18, p=0.80).

To test the role of medial septum (MS) cholinergic neurons in controlling IIS we crossed female homozygous choline acetyltransferase (ChAT) ChAT-Cre$^{+/+}$ mice[39] (Jax stock #006410) to male Tg2576 transgenic mice. This cross was used to allow the selective expression of viral vectors in MS cholinergic neurons as per previous studies.[40-42] We used 4 ChAT-Cre::Tg2576 transgenic mice and their ages were 9.6±3.6 months-old (range 3-16 months).

Presenilin 2 knockout (PS2KO) mice (n=4 controls; n=5 transgenic) were used because mutations in the *PS2* gene occur in a form of familial AD with early onset.[43] PS2KO transgenic mice do not develop Aβ neuropathology[44] which allowed us to study IIS independent of it. PS2KO mice were 10.7±1.9 months-old (range 6-15 months) at the time of recording. PS2KO control mice were 10.7±1.9 months-old (range 6-15 months). No statistically significant age differences were found between control and transgenic PS2KO mice (unpaired t-test, t=0.009, df=6, p=0.99).

The Ts65Dn model (n=5 controls; n=3 transgenic) of Down's syndrome has a triplicated portion of the mouse chromosome 16 containing the *APP* gene.[45] Ts65Dn mice show neuronal degeneration in the cholinergic neurons of the basal forebrain, like human AD.[45] Ts65Dn transgenic mice were 15.6±3.0 months-old (range 3-24 months) at the time of recording and Ts65Dn control mice were 15.3±4.6 months-old (range 3-24 months). No statistically significant differences were found between control and transgenic Ts65Dn mice (Mann-Whitney *U*-test, U=20.5, p=0.82). There were no statistically significant differences in age between the controls of different mouse lines (Kruskal-Wallis test, H(3)=3.89, p=0.14) and no differences in transgenics of the different mouse lines (Kruskal-Wallis test, H(3)=4.84, p=0.08).

II. Medial septum viral injections

Three weeks before the chemogenetic experiments ChAT-Cre::Tg2576 mice were anesthetized with 3% isoflurane and then transferred to a stereotaxic apparatus where anesthesia was maintained with 1-2% isoflurane. Mice were placed on a heating pad (#50-7220F, Harvard Apparatus) with a rectal probe for control of body temperature. Next, buprenorphine (0.05 mg/kg) was injected subcutaneously (s.c.) to reduce discomfort. One burr hole was drilled above the MS (+0.7 mm Anterior-Posterior; A-P 0 mm Medio-Lateral; M-L) and 500 nL of adeno-associated virus containing a modified designer receptor (hM4D) carrying an inhibitory signaling cascade (Gi; AAV5-hSyn-DIO-hM4D(Gi)-mCherry, Addgene) was stereotaxically injected over 10 min into the MS (-3.5 mm Dorso-Ventral; D-V, measured from the surface of the dura as before[46]). The needle was then left in place for another 10 min and it was slowly retracted to avoid backflow of the injected virus. During the same surgery, one depth electrode was implanted in the left DG following procedures described below. Chemogenetic experiments were conducted 3 weeks after EEG surgery to allow for sufficient expression of the injected virus and recovery from EEG surgery.

III. Electrode implantation

Mice were anesthetized with 3% isoflurane and then placed in a stereotaxic apparatus where anesthesia was maintained with 1-2% isoflurane and body temperature controlled as described above. Next, buprenorphine (0.05 mg/kg, s.c.) was injected to reduce discomfort. Two burr holes were drilled above the cerebellum and subdural screw electrodes (2.54 mm length stainless steel, JI Morris) were placed and stabilized using dental cement (Lang Dental) to serve as a reference (-5.7 mm A-P, +1.25 mm M-L) and a ground (-5.7 mm A-P, -1.25 mm M-L). Next, a burr hole was drilled over the left hippocampus (-1.9 mm A-P, -1.2 mm M-L) and one 16-channel silicon probe (#A1x16, Neuronexus or #PLX-QP-3-16E-v2, Plexon) was implanted in the left dorsal DG (-1.9 mm A-P, -1.2 mm M-L, -1.9 mm D-V). The mice used for chemogenetic experiments were implanted with a single wire (instead of a silicone probe) in the left dorsal DG (-1.9 mm A-P, -1.2 mm M-L, -1.9 mm D-V). The single wire was 90 µm diameter stainless steel (California Fine Wire).

IV. Wideband electrophysiological recordings

For EEG recording, mice were housed in a 21 cm x 19 cm square transparent plexiglass cage with access to food and water. A pre-amplifier (#C3335, Intan Techologies) was connected to the probe connector or the headset (in the case of mice recorded with a single wire) and then to a rotatory joint (Doric Lenses) via a lightweight cable to allow unrestricted movement of the mouse.

EEG signals were recorded at 2 kHz sampling rate using a bandpass filter (0.1-500 Hz) with either the Digital Lynx SX (Neuralynx) or an RHD interface board (#C3100, Intan Techologies) using the same settings. High frame rate video (>30 frames/sec) was recorded simultaneously using an infrared camera (#ac2000, Basler). Mice were continuously recorded for 3 consecutive days at a minimum.

V. Chemogenetic silencing of MS cholinergic neurons

For chemogenetic silencing of hM4D(Gi)-expressing MS cholinergic neurons and their axons, mice were injected intraperitoneally (i.p.) with CNO (3 mg/kg diluted in sterile saline; #BML-NS105-0005, Enzo Life Sciences) to activate the inhibitory Designer Receptors Exclusively Activated by Designer Drugs (iDREADDs). The CNO solution was made fresh before the start of each experiment. In presence of CNO, hM4D(Gi) activates inward rectifying potassium channels that hyperpolarize hM4D(Gi)-expressing cells.[47] We used a 3 mg/kg dose of CNO because it is a standard dose used in the literature to inhibit diverse cell types with minimal to no off-target effects.[48-50]

Previous studies in mice have shown that blood plasma[51] and brain[50] levels of CNO peak within 30 min after CNO injection, and the observed effects may last for hrs.[52] Thus, we injected CNO only once and analyzed effects for the next one hour following the 30 min waiting period necessary

for CNO levels to peak in plasma and brain. Notably, the mice were handled daily and were well-acclimated to the experimenter thus they did not show any signs of behavioral stress after injection that would likely influence the experiments.

VI. IIS detection and IIS amplitude analysis

IIS were detected using the same criteria as described in our previous studies.[11,14,53] In brief, we included IIS that exceeded the mean baseline by more than 5 standard deviations (SDs) during the same behavioral state.

For non-chemogenetic experiments we analyzed IIS during a 24 hr recording period. During the 24 hr period, we noted which IIS occurred during wakefulness, slow-wave sleep (SWS) or rapid eye movement (REM) sleep. Sleep stages were determined using the same criteria as in our previous studies.[14,46] The frequency of IIS per min is reported separately for each behavioral state investigated (wakefulness, SWS, REM sleep). For spectral analyses, we used the time-frequency function in the RippleLab MATLAB application[54] and applied a 64-point window to visualize spectral power in the 0–15 Hz frequency range.

For MS chemogenetic experiments, IIS were detected using the same threshold as mentioned above (i.e., 5 SDs above the mean). Baseline IIS frequency was calculated during two 1 hr-long recording periods preceding the CNO injection and the mean number of IIS per hr is reported. After CNO injection, a 30 min recording period was excluded from IIS analyses to allow enough time for CNO levels to peak in the plasma and brain.[50,51] After the 30 min waiting period following CNO injection, IIS were quantified from an 1 hr-long recording period.

To quantify IIS amplitude across different recording channels (for Figs 4-6), the amplitude of IIS was measured at the time that IIS reached its maximum amplitude after crossing the detection threshold (defined above). IIS amplitude was measured for all detected IIS occurring within the 24 hr recording period. IIS amplitude measurements were done separately for each recording channel. We report the mean ± standard error of the mean (SEM) of IIS amplitude per recording channel as a mean per animal.

To determine the position of each electrode relative to the cell layers we used the same electrophysiological landmarks as in our prior study.[14] In brief, the CA1 pyramidal layer was identified by predominance of ripple oscillations in the 80-200 Hz frequency range.[55] The CA1 stratum radiatum was defined by the occurrence of sharp waves.[56] Electrodes in the DG were identified by the robust presence of fast activity in the gamma (~80-150 Hz) frequency range[57] and in those DG channels the GCL was identified by the presence of multiunit activity.

VII. Histology

Mice were deeply anesthetized with isoflurane and then injected with an overdose of urethane (2.5 g/kg, i.p., Sigma Aldrich). Mice were transcardially perfused with 10 ml of room temperature (25 °C) saline, followed by 30 ml of cold (4 °C) 4% paraformaldehyde (Sigma Aldrich) dissolved in 0.1 M phosphate buffer (pH = 7.4). The brain was quickly removed and stored overnight in 4% paraformaldehyde. Coronal brain sections (50 μm) were cut using a vibratome (#Vibratome 3000, Ted Pella) and stored in cryoprotectant solution at 4 °C until use.

For Nissl stain, sections were mounted on 3% gelatin-coated slides and allowed to dry overnight. Then slides were dehydrated in increasing concentrations of ethanol (70%, 95%, 100%, 100%) for 2.5 min each, cleared in Xylene (Sigma Aldrich), and dehydrated again (100%, 100%, 95%, 70%) followed by hydration in double-distilled (dd) H_20 for 30 sec. Then sections were stained with 0.25% cresyl violet (Sigma Aldrich) in ddH_20 for 1.5 min followed by 30 sec in 4% acetic acid. Next, sections were dehydrated (70%, 95%, 100%, 100%), cleared in Xylene, and cover-slipped with Permount (Electron Microscopy Systems). Electrode placement was imaged using a microscope (#BX51, Olympus of America) equipped with a digital camera (#Infinity3-6URC, Olympus of America) at 2752x2192 pixel resolution and Infinity capture software (Olympus of America). The position of all

electrodes was verified and reported in supplemental figures 2-4 of Lisgaras and Scharfman 2022.[14] An additional representative example of electrode targeting is shown in Fig 1B.

To verify the success of AAV5-hSyn-DIO-hM4D(Gi)-mCherry viral expression in MS, 3 coronal brain sections adjacent to MS injection site (approximately +0.6 to +0.8 mm A-P, 0 M-L, -3.5 mm D-V) were mounted on 3% gelatin-coated slides and allowed to dry overnight. Then, the slides were coverslipped with Citifluor antifade mounting medium (Electron Microscopy Sciences) and micrographs were acquired using an epifluorescence microscope (#BX51, Olympus of America) with a digital camera (#Infinity3-6URC, Olympus of America) and Infinity capture software (Olympus of America). We visualized AAV5-hSyn-DIO-hM4D(Gi)-mCherry expression using mCherry fluorescence tag in the MS of ChAT-Cre::Tg2576 mice where Cre recombinase is known to be expressed in ChAT+ neurons.[40-42] We found robust AAV5-hSyn-DIO-hM4D(Gi)-mCherry expression in MS in all 4 mice we injected (typically 10-20 labeled cells per section). We also assessed whether expression occurred in areas outside MS such as in neighboring lateral septum and we did not detect expression there as shown in a representative example in Fig 3C.

VIII. Statistics

Data are presented as a mean ± SEM. Dots indicate individual data points. Statistical significance was set at $p<0.05$ and is denoted by asterisks on all graphs. Statistical comparisons that did not reach significance are not designated by a symbol in graphs but are reported in text.

All statistical analyses were performed using Prism (Graphpad). To determine if data fit a normal distribution, the Shapiro-Wilk test was used. Comparisons of parametric data of two groups were conducted using unpaired two-tailed t-tests or paired two-tailed t-tests. When data did not fit a normal distribution, non-parametric statistics were used. The non-parametric test to compare two groups was the Mann-Whitney *U*-test. For comparisons of more than 2 groups, one-way ANOVA was used when data were parametric and Kruskal-Wallis for non-parametric data. When a statistically significant main effect was found by ANOVA, Bonferroni *post-hoc* tests were used with corrections for multiple comparisons and for Kruskal-Wallis, Dunn's *post-hoc* tests were used.

RESULTS

I. IIS is a common EEG abnormality in three mouse models of AD

To test whether IIS were robust in different mouse models of AD, mice were implanted with electrodes and after 1 week of recovery they were video-EEG recorded continuously for 3 consecutive days (Fig 1A1-2). We used 3 different mouse models of AD, each with a different causal mechanism and neuropathology (see Methods). For all AD models, age-matched controls (n=14) were recorded alongside the transgenic mice (n=14). A representative Nissl-stained section confirming electrode targeting in the DG is shown in Fig 1B. Representative EEG examples from both the control and transgenic mice are shown in Fig 1C-E.

We found that all transgenic mice showed IIS (n=6 Tg2576, n=5 PS2KO, n=3 Ts65Dn). An IIS recorded in a Tg2576 transgenic mouse is shown in Fig 1C2 and further expanded in time in the inset. PS2KO and Ts65Dn mice also showed IIS and representative examples are shown in Fig 1D2 and Fig 1E2, respectively. We found that none of the age-matched controls showed IIS (n=5 Tg2576, n=4 PS2KO, n=5 Ts65Dn; Fig 1C1, 1D1, 1E1, respectively). Thus, IIS were an EEG event in transgenic mice not the controls, and therefore were an abnormal electrical pattern.

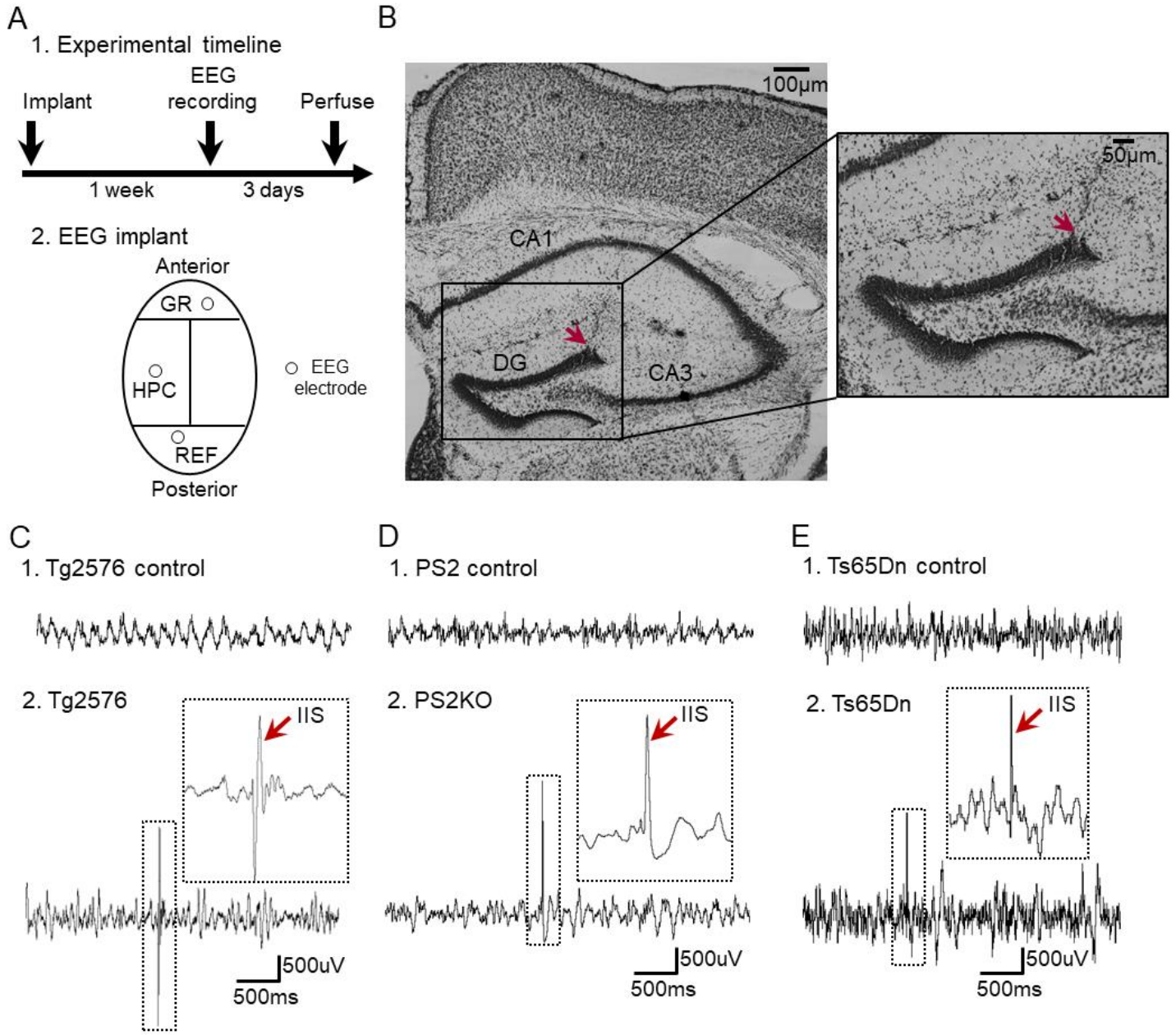

Figure 1: IIS is a robust EEG abnormality in three mouse models of AD

(A) A1. Experimental timeline of the study. Mice were implanted with a 16-channel silicon probe or a depth electrode and were allowed to recover from surgery for 1 week before the start of the video-EEG recording. Following 1 week of recovery, video-EEG recording began and lasted for 3 consecutive days. After the end of the video-EEG recording, animals were euthanized.
A2 shows a diagram of the implant used for the EEG recordings. HPC=hippocampus; GR=ground; REF=reference. For simplicity, only one EEG channel is shown for each mouse and the channel was in the DG.

(B) A representative Nissl-stained section confirming electrode targeting in the dentate gyrus (DG; red arrow) of the hippocampus.

(C) Representative examples of EEG recordings in the DG of a Tg2576 control and transgenic mouse.
C1 shows EEG in a control mouse. Note the absence of IIS. IIS were absent in all 5 control mice.

C2 is the same as C1 but the mouse was a Tg2576. An IIS is shown (red arrow) and it is further expanded in the inset. All 6 Tg2576 mice showed IIS.

(D) Representative examples of EEG recordings in the DG of a PS2KO control and transgenic mouse. D1 shows EEG in a control mouse. Note the absence of IIS. IIS were absent in all 4 control mice. D2 is the same as D1 but the mouse was a PS2KO. An IIS is shown (red arrow) and it is further expanded in the inset. All 5 PS2KO mice showed IIS.

(E) Representative examples of EEG recordings in the DG of a Ts65Dn control and transgenic mouse.
E1 shows EEG in a control mouse. Note the absence of IIS. IIS were absent in all 5 control mice. E2 is the same as E1 but the mouse was a Ts65Dn. An IIS is shown (red arrow) and it is further expanded in the inset. All 3 Ts65Dn mice showed IIS.

II. IIS in three AD models are robust during REM sleep

We next asked when IIS occurred in the AD models. We analyzed IIS during different behavioral states including wakefulness and sleep. Wakefulness included times when mice were awake and immobile and times when they were actively exploring their home cage. Sleep was divided into SWS and REM using an elevated theta/delta ratio to define REM, as in our previous studies.[11,14,46]

In all transgenic mice (n=14; n=6 Tg2576, n=5 PS2KO, n=3 Ts65Dn) IIS occurred during REM sleep (Fig 2A) and were absent during wakefulness (Fig 2B) or SWS (Fig 2C). None of the controls (n=14; n=5 Tg2576, n=4 PS2KO, n=5 Ts65Dn) showed IIS in any behavioral state (Fig 2B-D).

We next compared IIS frequency between the different mouse lines. Kruskal-Wallis test revealed that IIS frequency was significantly different between mouse lines during REM sleep (Kruskal-Wallis test, $H(3)=9.64$, $p=0.001$; Fig 2D). *Post-hoc* comparisons confirmed that IIS frequency was significantly higher in Tg2576 transgenic mice vs. PS2KO ($p=0.01$; Fig 2D) or Ts65Dn ($p=0.04$; Fig 2D) transgenic mice.

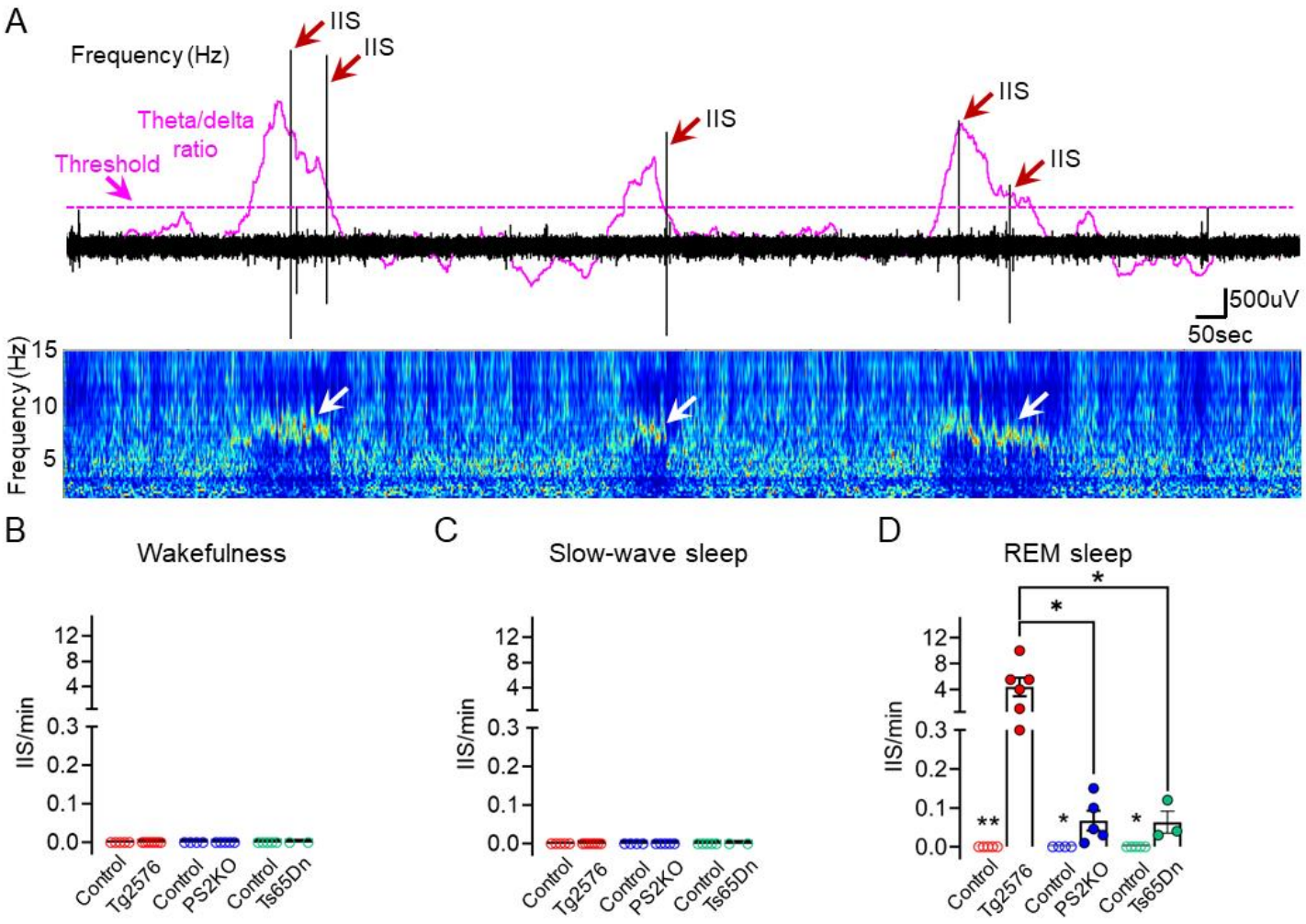

Figure 2: IIS frequency is significantly increased during REM sleep

(A) Theta/delta ratio (purple line) and IIS (red arrows) in a Tg2576 transgenic mouse during sleep. The threshold for sleep periods of increased (2 times above the baseline) theta/delta ratio is denoted by a dotted purple line. Note that IIS occurred during periods of theta/delta ratio exceeding the threshold which are consistent with REM sleep. Also note the increased theta power (white arrows) in the spectrogram during periods when IIS occurred.

(B) IIS frequency during wakefulness. None of the transgenic or control mice showed IIS during wakefulness. Red denotes Tg2576 control (n=5) and transgenic (n=6) mice. Blue denotes PS2KO control (n=4) and transgenic (n=5) mice, and green Ts65Dn control (n=5) and transgenic (n=3) mice.

(C) Same as in B but for SWS sleep. None of the transgenic or control mice showed IIS.

(D) Same as in C but IIS were analyzed during REM sleep. IIS in Tg2576 transgenic mice were most frequent compared to PS2KO (p=0.01) or Ts65Dn (p=0.04) transgenic mice. Note than none of the controls showed IIS (n=14). Also, IIS were significantly more frequent in Tg2576 transgenic vs. control mice (Mann-Whitney *U*-test, U=0, p=0.004), PS2KO transgenic vs. control mice (Mann-Whitney *U*-test, U=0, p=0.01) and Ts65Dn transgenic vs. control mice (Mann-Whitney *U*-test, U=0, p=0.01).

III. Selective chemogenetic silencing of MS cholinergic neurons significantly reduced IIS

IIS occurred during REM sleep, a sleep period when MS cholinergic tone is increased compared to SWS or wakefulness.[26,27] We thus asked whether IIS frequency would be affected if we silenced MS cholinergic neurons. To test this hypothesis, we used Tg2576 transgenic mice because they show significantly more IIS compared to PS2KO or Ts65Dn transgenic mice (Fig 2D). Tg2576 transgenic mice were crossed to ChAT-Cre homozygous mice so that offspring mice would selectively express Cre recombinase in MS cholinergic neurons.[39-42] Next, ChAT-Cre::Tg2576 mice were injected with AAV5-hSyn-DIO-hM4D(Gi)-mCherry in MS and a depth electrode was implanted in the DG (Fig 3A). Next, we asked whether selective chemogenetic silencing of MS cholinergic neurons would be sufficient to reduce the number of IIS. Thus, we used an acute chemogenetic silencing approach (Fig 3B) where ChAT-Cre::Tg2576 mice were recorded for a 2 hr-long baseline period and the number of IIS per hr was determined. Next, the mice were injected i.p. with a 3 mg/kg dose of CNO. Immediately after a 30 min waiting period post-CNO injection, which is necessary for CNO to peak in the brain,[50] EEG was recorded for the next 1 hr. The number of IIS per hr was determined for this recording period.

We first verified the success of AAV5-hSyn-DIO-hM4D(Gi)-mCherry expression in MS (see Methods) and a representative example of AAV5-hSyn-DIO-hM4D(Gi)-mCherry expression is shown in Fig 3C. Fig 3D shows a representative baseline EEG recording with IIS. Note that IIS occurred when theta/delta ratio was above the threshold that we used to define REM sleep (dotted line in Fig 3D-E). We found that within the 1 hr after CNO injection, the number of IIS occurring during REM sleep was markedly reduced (Fig 3E). We quantified this effect and found that the total number of IIS per hr was significantly lower within the 1 hr following CNO injection vs. baseline (paired t-test, t_{crit}=4.59, p=0.01; Fig 3F1, n=4 mice). Indeed, during the 1 hr recording period (starting 30 min after CNO injection), the number of IIS was reduced by 68.1±2.8% (n=4 mice) compared to baseline (Fig 3F2).

We next asked whether the reduction in the number of IIS could be explained by any effects on REM sleep characteristics such as duration or number of bouts. We thus compared the total duration of REM sleep between the two recording periods (the 1 hr baseline vs. the 1 hr starting 30 min after CNO). We found no statistically significant differences in total duration of REM sleep (Wilcoxon signed rank test, p=0.87; Fig 3G1). Similarly, we did not find any statistically significant differences in the number of REM bouts (paired t-test, t_{crit}=0.52, p=0.63; Fig 3G2) or the duration of REM bouts (Wilcoxon signed rank test, p=0.91; Fig 3G3) between baseline and 1 hr post-CNO injection.

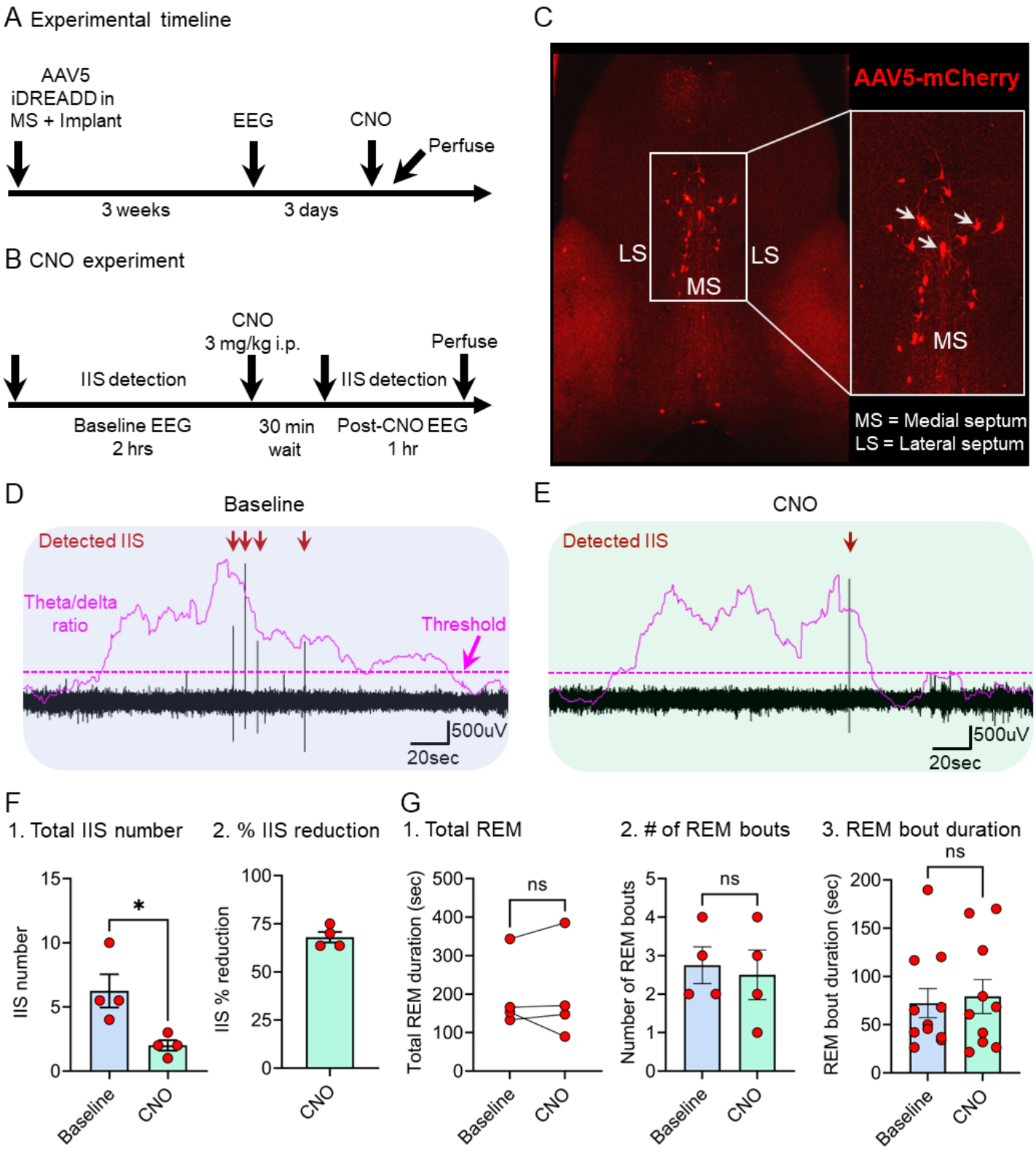

Figure 3: IIS are significantly reduced by selective chemogenetic silencing of MS cholinergic neurons

(A) Experimental timeline of the study. ChAT-Cre::Tg2576 mice were injected with AAV5-hSyn-DIO-hM4D(Gi)-mCherry in MS and in the same surgery mice were implanted with a depth electrode in the DG. After 3 weeks to allow for expression of the virus and recovery from the EEG surgery,

mice were video-EEG recorded continuously for 3 consecutive days and then the CNO experiment followed. Afterwards, mice were euthanized.

(B) Timeline of the acute CNO experiment. A 2 hr-long baseline EEG was recorded and then 3 mg/kg CNO was injected i.p. After waiting for 30 min, we counted IIS for the next hr and afterwards the mice were euthanized.

(C) Representative viral expression of AAV5-hSyn-DIO-hM4D(Gi)-mCherry in MS of a ChAT-Cre::Tg2576 mouse. Inset shows MS at higher magnification and white arrows point to individual cells expressing AAV5-hSyn-DIO-hM4D(Gi)-mCherry. MS = Medial septum, LS = Lateral septum.

(D) Representative example of video-EEG recorded for a baseline. Theta/delta ratio is shown in purple and detected IIS are noted with a red arrow. Note that IIS occurred during a period of increased theta/delta ratio shown by a purple dotted line.

(E) In the same mouse as D, CNO was injected, and the recording is shown after waiting 30 min for CNO to reach stable brain levels.

(F) Note the reduced number of IIS occurring during periods of increased theta/delta ratio.

1. The total number of IIS occurring during baseline and during the 1 hr after CNO injection are compared. The total number of IIS was significantly reduced post-CNO vs. baseline (paired t-test, t_{crit}=4.59, p=0.01).

2. The percent decrease in the total IIS number post-CNO vs. baseline is shown. The total number of IIS during 1 hr post-CNO was reduced by 68.1±2.8% compared to baseline.

(G) Characteristics of REM sleep during the baseline and 1 hr recording period that started 30 min following CNO injection.

1. The total duration of REM sleep during the baseline and 1 hr post-CNO injection is shown. We found no statistically significant differences in the total duration of REM sleep between baseline and post-CNO (Wilcoxon signed rank test, p=0.87). ns, not significant.

2. The number of REM sleep bouts is shown. We found no statistically significantly differences between baseline and post-CNO (paired t-test, t_{crit}=0.52, p=0.63).

3. The same as G2, but REM bout duration is shown. No statistically significant differences were found for REM bout duration between baseline and 1 hr post-CNO injection (Wilcoxon signed rank test, p=0.91).

IV. IIS in AD models show an amplitude gradient along the cortical-CA1-DG axis and maximal amplitude within the DG

To test whether there was a location along the cortical-CA1-DG axis where IIS were consistently maximal, transgenic mice were implanted with a multi-channel linear silicon probe with the tip ending in the dorsal DG. The silicon probe spanned the cortical-CA1-DG axis allowing simultaneous recordings of IIS in the DG, CA1 and overlying cortical layers.

A representative example of an IIS recorded from a Tg2576 transgenic mouse is shown in Fig 4A. We found that IIS were detectable throughout the cortical-CA1-DG axis. Insets show IIS recorded in the DG GCL, CA1 pyramidal layer or a deep cortical layer. One-way ANOVA analysis revealed a statistically significant difference of IIS amplitudes for the different recording channels (F(14, 30)=2.43, p=0.02, n=4 mice; Fig 4B). *Post-hoc* comparisons confirmed that IIS amplitude was significantly larger in the DG GCL vs. CA1 stratum radiatum (p=0.003; Fig 4B), CA1 pyramidal cell layer (p=0.0003; Fig 4B) or deep cortical layers (p=0.0004; Fig 4B).

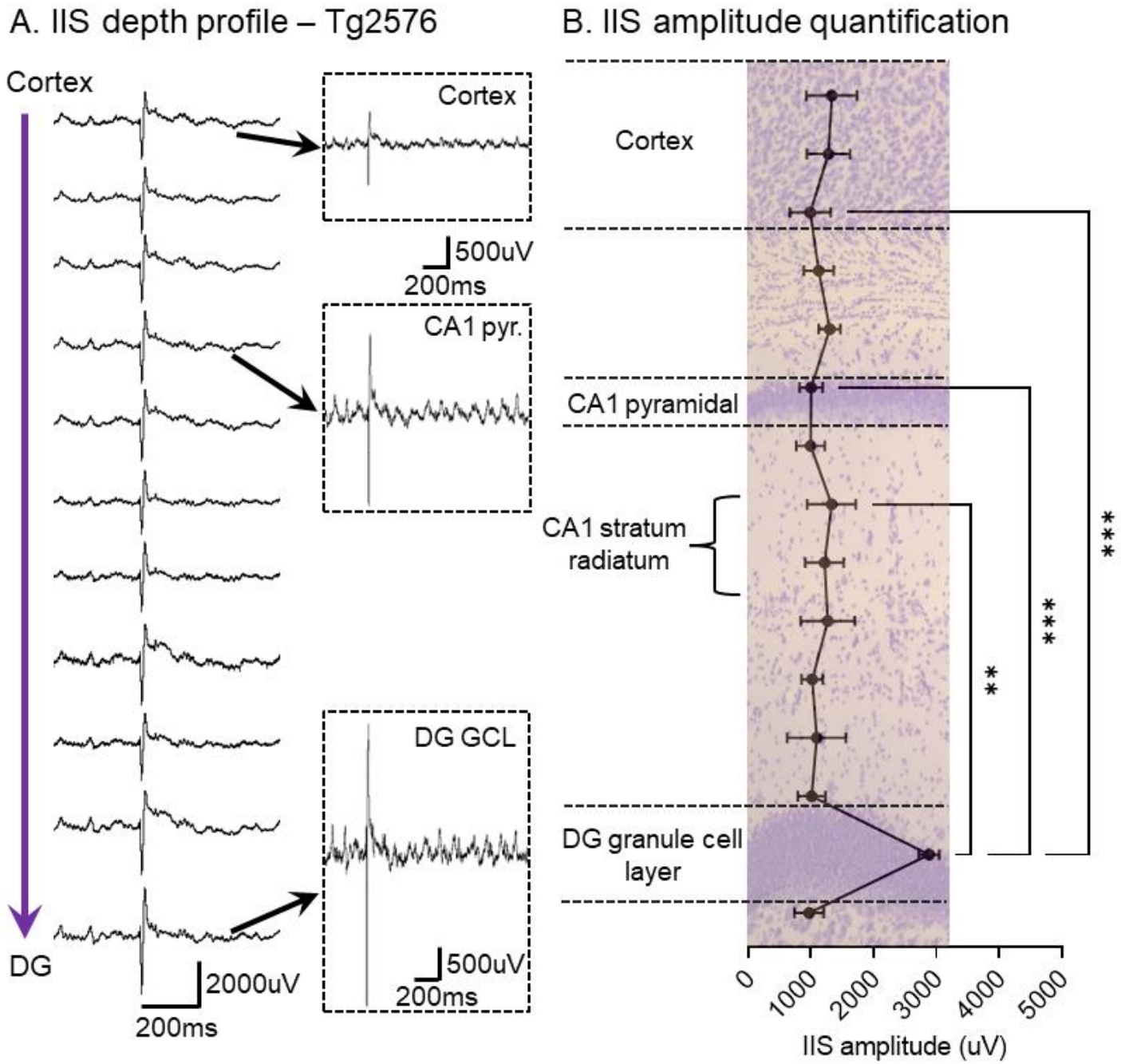

Figure 4: IIS amplitude is maximal in the DG of Tg2576 transgenic mice

(A) A representative IIS recorded from a Tg2576 transgenic mouse. The recording channels are shown with the most superficial (closer to cortex) at the top and deeper channels (closer to the DG) at the bottom. Note that the IIS was detectable from all recording channels. Insets show an IIS in a deep cortical layer (top), CA1 pyramidal layer (center) and the DG GCL (bottom).

(B) Quantification of IIS amplitude along the cortical-CA1-DG axis of Tg2576 transgenic mice (n=4 mice). The different layers were determined based on electrophysiological landmarks such as predominance of ripple oscillations (80-200 Hz) in CA1 pyramidal layer and large gamma oscillations (~80-150 Hz) in the DG GCL (for details see Methods). One-way ANOVA revealed a statistically significant difference in IIS amplitudes for different recording channels ($F(14, 30)=2.43$, $p=0.02$). *Post-hoc* comparisons confirmed that IIS amplitude was significantly larger in the DG GCL vs. CA1 stratum radiatum ($p=0.003$), CA1 pyramidal cell layer ($p=0.0003$) or deep cortical layers ($p=0.0004$).

We next asked whether the maximal IIS amplitude in the GCL of Tg2576 transgenic mice was generalizable to other AD mouse models. To that end, we implanted PS2KO transgenic mice and we found that IIS in REM sleep also showed a statistically significant amplitude gradient along the cortical-CA1-DG axis (Kruskal-Wallis test, H(13)=22.84, p=0.02, n=4 mice; Fig 5A). *Post-hoc* comparisons, confirmed that IIS amplitude was significantly larger in the GCL compared to CA1 pyramidal layer (p=0.01; Fig 5B) or deep cortical layers (p=0.02; Fig 5B).

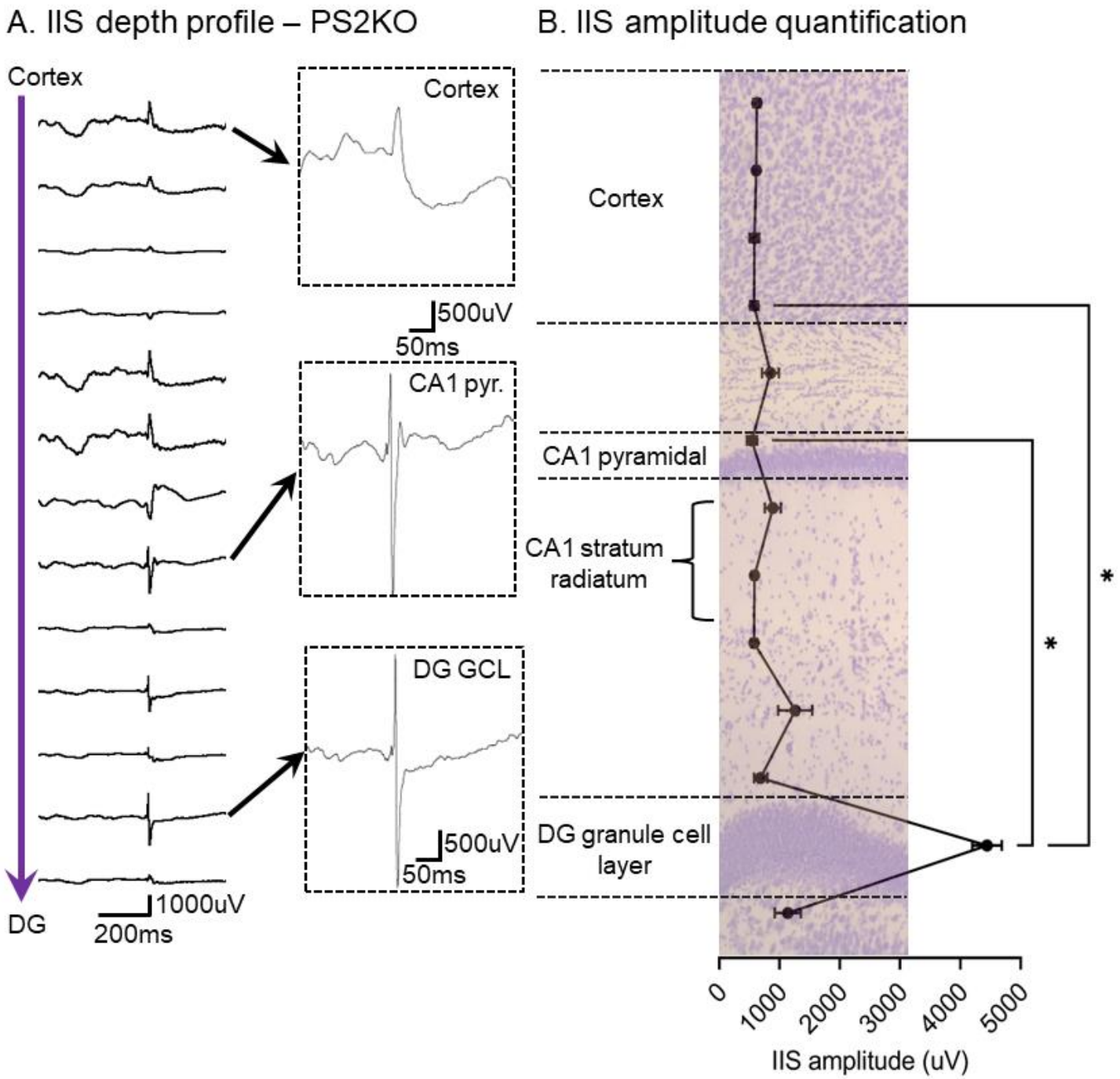

Figure 5: IIS amplitude is maximal in the DG of PS2KO transgenic mice

(A) A representative IIS recorded from a PS2KO mouse is shown. Similar to Tg2576 transgenic mice, IIS in PS2KO transgenic mice were detectable from all recording channels. Insets show an IIS in a deep cortical layer (top), CA1 pyramidal layer (center) and the DG GCL (bottom).

(B) Quantification of IIS amplitude along the cortical-CA1-DG axis of PS2KO mice (n=4 mice). One-way ANOVA analysis revealed a statistically significant difference for IIS amplitude and recording channel (Kruskal-Wallis test, H(13)=22.84, p=0.02). *Post-hoc* comparisons confirmed that IIS amplitude was significantly larger in the GCL vs. CA1 pyramidal cell layer (p=0.01) or deep cortical layers (p=0.02).

In a third mouse model of AD, the Ts65Dn mouse, we also found a statistically significant IIS amplitude gradient along the cortical-CA1-DG axis (Friedman test (12)=25.85, p=0.007, n=3 mice; Fig 6A-B). *Post-hoc* comparisons revealed a significant increase in IIS amplitude in the GCL vs. CA1 pyramidal layer (p=0.04; Fig 6B) or deep cortical layers (p=0.03; Fig 6B).

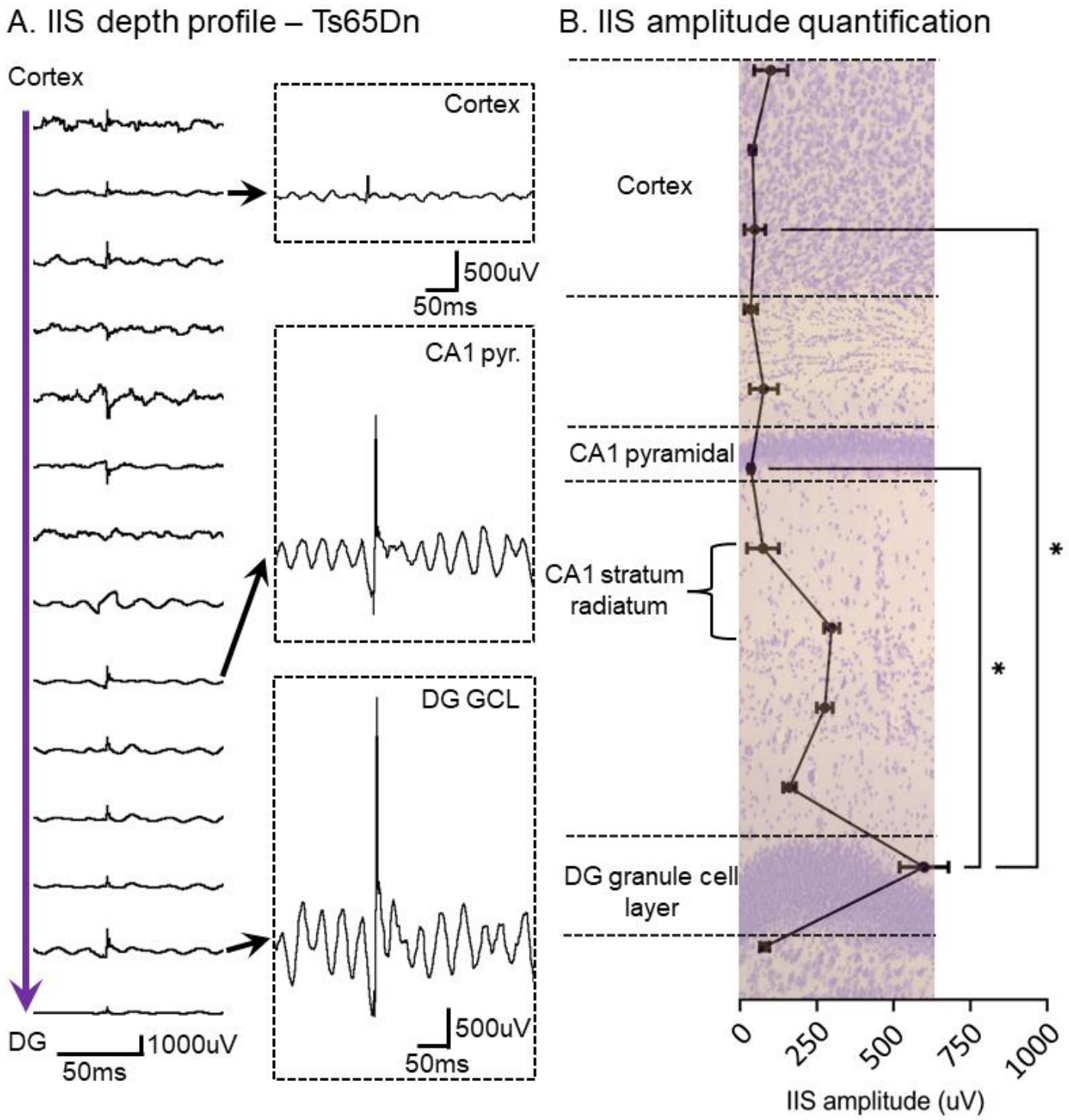

Figure 6: IIS amplitude is maximal in the DG of Ts65Dn transgenic mice

(A) A representative IIS recorded in a Ts65Dn mouse is shown. Like Tg2576 and PS2KO mice, IIS in Ts65Dn mice were detectable from all recording channels. Insets show IIS in a deep cortical layer (top), CA1 pyramidal layer (center) and the GCL (bottom).

(B) Quantification of IIS amplitude along the cortical-CA1-DG axis of Ts65Dn transgenic mice (n=3 mice). Friedman test revealed a statistically significant difference for IIS amplitude and recording channel (Friedman test(12)=25.85, p=0.007). *Post-hoc* comparisons confirmed that IIS amplitude was significantly larger in the GCL vs. CA1 pyramidal cell layer (p=0.04) or deep cortical layers (p=0.03).

DISCUSSION

Summary of main findings

The goal of this study was to understand where IIS are most robust in AD models and the role of MS cholinergic neurons in controlling IIS. We found that IIS is a robust EEG abnormality in 3 mouse models of AD. We also found that IIS occurred primarily in REM sleep. Using chemogenetics, we confirmed that selective silencing of MS cholinergic neurons reduced IIS frequency. In addition, multi-channel EEG recordings revealed that IIS amplitude was maximal in the GCL relative to area CA1 and overlying cortex. Our findings provide substantial insight into the possible areas generating IIS in AD models. We also provide novel evidence for a contributing role of MS cholinergic neurons in IIS generation which may serve as a new strategy to abate IIS in AD models.

IIS represent a common EEG disturbance in different AD mouse models

We found that IIS occurred in all transgenic mice but not in the controls. Although IIS are known to occur in Tg2576 transgenic mice,[11,14] their origin was unclear and it was also unclear whether PS2KO and Ts65Dn transgenic mice would show robust IIS.

PS2KO transgenic mice are characterized by a lower seizure threshold when seizures are triggered using the kindling paradigm[13] but spontaneous epileptiform activity has not been reported to date. Therefore, showing PS2KO mice have IIS is novel. It is also possible that IIS contribute to higher seizure susceptibility of these mice. However, IIS in epilepsy are not always considered pro-excitatory.[58-60] One additional spontaneous event we reported recently in PS2KO mice are HFOs [14] Thus, PS2KO mice show two types of spontaneous abnormalities in the EEG, supporting the view that the mice have hyperexcitability. That is interesting in light of the clinical findings of *PS2* mutations in AD, where hyperexcitability has been reported.[43,61,62]

The Ts65Dn transgenic mice we recorded also showed robust IIS which has not been reported before. Taken together, the presence of robust IIS in 3 AD models suggests that IIS can arise for multiple reasons, consistent with epilepsy where IIS occur in diverse types of epilepsy. The results also suggest that IIS could be a promising EEG signature to consider as an outcome measure in AD. IIS could also be a possible treatment target in AD.[43]

IIS were most frequent in Tg2576 transgenic mice

Among all 3 AD mouse models we examined, we found that IIS were most frequent in Tg2576 transgenic mice. More frequent IIS in Tg2576 mice (vs. PS2KO or Ts65Dn mice) is reminiscent of the higher frequency of spontaneous HFOs in Tg2576 mice we reported previously.[14] Thus, both increased frequency of IIS and HFOs in Tg2576 mice may be related to plaque burden[36] which is high in Tg2576 mice but not in PS2KO[44] and Ts65Dn[45] mice. This idea is consistent with increased calcium transients in neurons around plaques.[63] However, IIS and HFOs can occur before plaques[11,14] so additional mechanisms may be involved.

Tg2576 transgenic mice are also known to experience seizures.[10,11,14] Thus, frequent IIS in Tg2576 transgenic mice may contribute to seizures in this model. That idea is consistent with a previous study using APP/PS1 transgenic mice which showed that IIS frequency correlated with a higher seizure burden.[12]

IIS during REM sleep and cholinergic control by medial septum

We found that IIS in AD models were robust in REM sleep. Acetylcholine (ACh) levels during REM sleep are increased to a greater extent compared to other behavioral states such as

wakefulness or SWS.[26,27] Thus, it is possible that increased ACh levels during REM sleep may facilitate the occurrence of IIS. Indeed cholinergic facilitation of IIS and seizures is known to occur in epilepsy.[28,29] In this context, our previous study has found that i.p. injection of the cholinergic antagonist atropine was effective in reducing IIS in REM as well as NREM (which primarily includes SWS).[11] However, the reduction of IIS in REM by atropine was confounded by a shortening of REM sleep duration after atropine administration. Also, the study[11] did not provide specificity for the involvement of MS cholinergic neurons as the current study.

The study using atropine prompted us to use an approach that would minimize effects on REM such as those related to reduced REM sleep duration. We chose an acute chemogenetic approach to interfere with cholinergic neurotransmission minimally by selectively targeting MS cholinergic neurons. Using this selective approach, we found that the number of IIS was significantly reduced without any significant effects in REM sleep duration or the number and duration of REM sleep bouts. These results suggest that selectively reducing MS cholinergic tone is sufficient in reducing IIS a finding that further support a role of MS cholinergic neurons in IIS generation.

Our data contrast with the widespread notion that cholinergic function should always be increased in AD.[64] This dominant view comes from observations of robust basal forebrain neurodegeneration which typically occurs late in AD progression.[34,35,64,65] Thus, the late degeneration of MS cholinergic neurons makes it appear that ACh levels are always too low in AD, and need to be increased. However, it has been shown that cholinergic markers like ChAT are high in mild cognitive impairment (MCI;[66]) and early AD.[67,68] In addition, increasing ACh using cholinesterase inhibitors like donezepil was not highly effective.[69,70] In our view, cholinergic activity may be elevated early and decay late in AD. Thus, silencing hyperactive MS cholinergic neurons in early AD may be beneficial. Silencing MS cholinergic neurons may also protect them from excessive activation and deterioration.

The DG as a possible source of IIS in AD models

Excitability in the DG is known to change early during AD progression. In amnestic MCI, fMRI showed high activity in the DG.[25] In AD mouse models, markers of neuronal activity such as c-Fos and delta FosB were elevated in the J20 mouse model in early life.[71] Reduced calbindin-D28K[72] and increased neuropeptide Y[8] in granule cells (GCs) of J20 mice is also consistent with hyperactive GCs. In vitro, slices of Tg2576 mice at 2-3 months of age showed increased excitability of GCs.[73] In vivo, we showed HFOs in the DG at just 1 month of age.[14]

Our study is the first to show that the DG dominates the activity that occurs during IIS. We showed that in all 3 AD models we tested IIS appeared to be maximal in amplitude in the GCL of the DG. A larger IIS amplitude would suggest that a greater number of neurons fire to produce an IIS compared to an IIS that is characterized by a smaller amplitude. Indeed, multiunit activity during IIS in epilepsy is found in brain areas where IIS are likely to be generated.[74,75] If that also is true in the context of AD, then larger IIS amplitude in the DG would suggest that the DG could be a possible area that contributes to IIS generation. Overall, these results suggest that the DG may contribute to a larger extent to IIS compared to either area CA1 or overlying cortex where IIS appear to occur with a significantly lower amplitude.

In the present study IIS amplitude gradually decreased dorsal to the GCL and that was the case in all 3 AD mouse models we studied. However, we cannot exclude the possibility that other areas we did not record from may also show robust IIS.

CONCLUSIONS

Showing that the DG is a location where IIS are consistently maximal in diverse AD models is important as it suggests the DG as a central node in the pathophysiology of AD.[76] This idea is consistent with many observations of altered excitability in the DG in AD[25] or AD mouse models.[8,71-73] Indeed, this view is also strengthened by our previous study showing that the DG is an early contributor to increased hippocampal excitability as shown by the occurrence of DG HFOs *in vivo*.[14] In addition, our findings pointing to the MS as a contributor to IIS activity is topical considering the urgent need for a better understanding of the role of subcortical structures in AD pathophysiology.[77] Future work targeting the DG as well as the MS is warranted as it may provide new avenues for therapeutic intervention in individuals at risk for developing AD.

ACKNOWLEDGEMENTS

We would like to thank Dr. Ralph Nixon for providing the PS2KO mice and Dr. Stephen Ginsberg for providing the Ts65Dn mice. This project was supported by NIH grants R01 AG-055328 and R01 NS-106983, and the New York State Office of Mental Health.

AUTHOR CONTRIBUTIONS

Conceptualization: CPL, HES
Data acquisition: CPL
Methodology: CPL
Data analysis: CPL
Funding acquisition: HES
Resources: HES
Project administration: HES
Supervision: HES
Data visualization: CPL, HES
Writing – original draft: CPL
Writing – review & editing: CPL, HES

CONFLICTS OF INTEREST/ETHICAL PUBLICATION STATEMENT

None of the authors has any conflict of interest to disclose. We confirm that we have read the Journal's position on issues involved in ethical publication and affirm that this report is consistent with those guidelines.

DATA AVAILABILITY STATEMENT

Data will be available from the corresponding author upon reasonable request.

REFERENCES

1. Palop JJ, Mucke L. Epilepsy and cognitive impairments in Alzheimer disease. Arch Neurol. 2009 Apr;66(4):435-40.

2. Scharfman HE. "Untangling" Alzheimer's disease and epilepsy. Epilepsy Curr. 2012 Sep;12(5):178-83.

3. Friedman D, Honig LS, Scarmeas N. Seizures and epilepsy in Alzheimer's disease. CNS Neurosci Ther. 2012 Apr;18(4):285-94.

4. Lam AD, Noebels J. Night Watch on the Titanic: Detecting early signs of epileptogenesis in Alzheimer disease. Epilepsy Curr. 2020 Nov-Dec;20(6):369-74.

5. Edwards M, Robertson NP. Seizures in Alzheimer’s disease: is there more beneath the surface? Journal of Neurology. 2018 2018/01/01;265(1):226-8.

6. Lam AD, Deck G, Goldman A, Eskandar EN, Noebels J, Cole AJ. Silent hippocampal seizures and spikes identified by foramen ovale electrodes in Alzheimer's disease. Nat Med. 2017 Jun;23(6):678-80.

7. Vossel KA, Tartaglia MC, Nygaard HB, Zeman AZ, Miller BL. Epileptic activity in Alzheimer's disease: causes and clinical relevance. Lancet Neurol. 2017 Apr;16(4):311-22.

8. Palop JJ, Chin J, Roberson ED, Wang J, Thwin MT, Bien-Ly N, Yoo J, Ho KO, Yu GQ, Kreitzer A, Finkbeiner S, Noebels JL, Mucke L. Aberrant excitatory neuronal activity and compensatory remodeling of inhibitory hippocampal circuits in mouse models of Alzheimer's disease. Neuron. 2007 Sep 6;55(5):697-711.

9. Minkeviciene R, Rheims S, Dobszay MB, Zilberter M, Hartikainen J, Fülöp L, Penke B, Zilberter Y, Harkany T, Pitkänen A, Tanila H. Amyloid beta-induced neuronal hyperexcitability triggers progressive epilepsy. J Neurosci. 2009 Mar 18;29(11):3453-62.

10. Bezzina C, Verret L, Juan C, Remaud J, Halley H, Rampon C, Dahan L. Early onset of hypersynchronous network activity and expression of a marker of chronic seizures in the Tg2576 mouse model of Alzheimer's disease. PLoS One. 2015;10(3):e0119910.

11. Kam K, Duffy AM, Moretto J, LaFrancois JJ, Scharfman HE. Interictal spikes during sleep are an early defect in the Tg2576 mouse model of beta-amyloid neuropathology. Sci Rep. 2016 Jan 28;6:20119.

12. Gureviciene I, Ishchenko I, Ziyatdinova S, Jin N, Lipponen A, Gurevicius K, Tanila H. Characterization of epileptic spiking associated with brain amyloidosis in APP/PS1 mice. Frontiers in Neurology. 2019 2019-November-12;10.

13. Beckman M, Knox K, Koneval Z, Smith C, Jayadev S, Barker-Haliski M. Loss of presenilin 2 age-dependently alters susceptibility to acute seizures and kindling acquisition. Neurobiol Dis. 2020 Mar;136:104719.

14. Lisgaras CP, Scharfman HE. High Frequency oscillations (250-500Hz) in animal models of Alzheimer's disease and two animal models of epilepsy. Epilepsia. 2022 Nov 8.

15. Scarmeas N, Honig LS, Choi H, Cantero J, Brandt J, Blacker D, Albert M, Amatniek JC, Marder K, Bell K, Hauser WA, Stern Y. Seizures in Alzheimer disease: who, when, and how common? Arch Neurol. 2009 Aug;66(8):992-7.

16. Vossel KA, Ranasinghe KG, Beagle AJ, Mizuiri D, Honma SM, Dowling AF, Darwish SM, Van Berlo V, Barnes DE, Mantle M, Karydas AM, Coppola G, Roberson ED, Miller BL, Garcia PA, Kirsch HE, Mucke L, Nagarajan SS. Incidence and impact of subclinical epileptiform activity in Alzheimer's disease. Annals of neurology. 2016;80(6):858-70.

17. Sperling RA, Jack CR, Jr., Aisen PS. Testing the right target and right drug at the right stage. Sci Transl Med. 2011 Nov 30;3(111):111cm33.

18. Kleen JK, Scott RC, Holmes GL, Lenck-Santini PP. Hippocampal interictal spikes disrupt cognition in rats. Ann Neurol. 2010 Feb;67(2):250-7.

19. Horak PC, Meisenhelter S, Song Y, Testorf ME, Kahana MJ, Viles WD, Bujarski KA, Connolly AC, Robbins AA, Sperling MR, Sharan AD, Worrell GA, Miller LR, Gross RE, Davis KA, Roberts DW, Lega B, Sheth SA, Zaghloul KA, Stein JM, Das SR, Rizzuto DS, Jobst BC. Interictal epileptiform discharges impair word recall in multiple brain areas. Epilepsia. 2017 Mar;58(3):373-80.

20. Sanchez PE, Zhu L, Verret L, Vossel KA, Orr AG, Cirrito JR, Devidze N, Ho K, Yu GQ, Palop JJ, Mucke L. Levetiracetam suppresses neuronal network dysfunction and reverses synaptic and cognitive deficits in an Alzheimer's disease model. Proc Natl Acad Sci U S A. 2012 Oct 16;109(42):E2895-903.

21. Horvath AA, Papp A, Zsuffa J, Szucs A, Luckl J, Radai F, Nagy F, Hidasi Z, Csukly G, Barcs G, Kamondi A. Subclinical epileptiform activity accelerates the progression of Alzheimer's disease: a long-term EEG study. Clin Neurophysiol. 2021 Aug;132(8):1982-9.

22. Vossel K, Ranasinghe KG, Beagle AJ, La A, Ah Pook K, Castro M, Mizuiri D, Honma SM, Venkateswaran N, Koestler M, Zhang W, Mucke L, Howell MJ, Possin KL, Kramer JH, Boxer AL, Miller BL, Nagarajan SS, Kirsch HE. Effect of levetiracetam on cognition in patients with

Alzheimer disease with and without epileptiform activity: a randomized clinical trial. JAMA Neurol. 2021 Nov 1;78(11):1345-54.

23. Stickgold R. Sleep-dependent memory consolidation. Nature. 2005 2005/10/01;437(7063):1272-8.

24. Vossel KA, Beagle AJ, Rabinovici GD, Shu H, Lee SE, Naasan G, Hegde M, Cornes SB, Henry ML, Nelson AB, Seeley WW, Geschwind MD, Gorno-Tempini ML, Shih T, Kirsch HE, Garcia PA, Miller BL, Mucke L. Seizures and epileptiform activity in the early stages of Alzheimer disease. JAMA Neurol. 2013 Sep 1;70(9):1158-66.

25. Bakker A, Krauss GL, Albert MS, Speck CL, Jones LR, Stark CE, Yassa MA, Bassett SS, Shelton AL, Gallagher M. Reduction of hippocampal hyperactivity improves cognition in amnestic mild cognitive impairment. Neuron. 2012 May 10;74(3):467-74.

26. Jasper HH, Tessier J. Acetylcholine liberation from cerebral cortex during paradoxical (REM) sleep. Science. 1971 May 7;172(3983):601-2.

27. Vazquez J, Baghdoyan HA. Basal forebrain acetylcholine release during REM sleep is significantly greater than during waking. American Journal of Physiology-Regulatory, Integrative and Comparative Physiology. 2001;280(2):R598-R601.

28. Friedman A, Behrens CJ, Heinemann U. Cholinergic dysfunction in temporal lobe epilepsy. Epilepsia. 2007;48 Suppl 5:126-30.

29. Mikroulis A, Lisgaras CP, Psarropoulou C. Immature status epilepticus: *in vitro* models reveal differences in cholinergic control and HFO properties of adult CA3 interictal discharges in temporal vs septal hippocampus. Neuroscience. 2018 Jan 15;369:386-98.

30. Hasselmo ME, Sarter M. Modes and models of forebrain cholinergic neuromodulation of cognition. Neuropsychopharmacology. 2011 Jan;36(1):52-73.

31. Zhang Y, Cao L, Varga V, Jing M, Karadas M, Li Y, Buzsáki G. Cholinergic suppression of hippocampal sharp-wave ripples impairs working memory. Proceedings of the National Academy of Sciences. 2021;118(15):e2016432118.

32. Hedreen JC, Struble RG, Whitehouse PJ, Price DL. Topography of the magnocellular basal forebrain system in human brain. J Neuropathol Exp Neurol. 1984 Jan;43(1):1-21.

33. Colom LV. Septal networks: relevance to theta rhythm, epilepsy and Alzheimer's disease. Journal of Neurochemistry. 2006;96(3):609-23.

34. Kim S, Nam Y, Jeong YO, Park HH, Lee SK, Shin SJ, Jung H, Kim BH, Hong SB, Park YH, Kim J, Yu J, Yoo DH, Park SH, Jeon SG, Moon M. Topographical visualization of the reciprocal projection between the medial septum and the hippocampus in the 5XFAD mouse Model of Alzheimer's Disease. Int J Mol Sci. 2019 Aug 16;20(16).

35. Falangola MF, Nie X, Ward R, Dhiman S, Voltin J, Nietert PJ, Jensen JH. Diffusion MRI detects basal forebrain cholinergic abnormalities in the 3xTg-AD mouse model of Alzheimer's disease. Magn Reson Imaging. 2021 Nov;83:1-13.

36. Hsiao K, Chapman P, Nilsen S, Eckman C, Harigaya Y, Younkin S, Yang F, Cole G. Correlative memory deficits, Abeta elevation, and amyloid plaques in transgenic mice. Science. 1996 Oct 4;274(5284):99-102.

37. Duffy AM, Morales-Corraliza J, Bermudez-Hernandez KM, Schaner MJ, Magagna-Poveda A, Mathews PM, Scharfman HE. Entorhinal cortical defects in Tg2576 mice are present as early as 2-4 months of age. Neurobiol Aging. 2015 Jan;36(1):134-48.

38. Ishii M, Wang G, Racchumi G, Dyke JP, Iadecola C. Transgenic mice overexpressing amyloid precursor protein exhibit early metabolic deficits and a pathologically low leptin state associated with hypothalamic dysfunction in arcuate neuropeptide Y neurons. J Neurosci. 2014 Jul 2;34(27):9096-106.

39. Rossi J, Balthasar N, Olson D, Scott M, Berglund E, Lee CE, Choi MJ, Lauzon D, Lowell BB, Elmquist JK. Melanocortin-4 receptors expressed by cholinergic neurons regulate energy balance and glucose homeostasis. Cell Metab. 2011 Feb 2;13(2):195-204.

40. Vandecasteele M, Varga V, Berényi A, Papp E, Barthó P, Venance L, Freund TF, Buzsáki G. Optogenetic activation of septal cholinergic neurons suppresses sharp wave ripples and enhances theta oscillations in the hippocampus. Proc Natl Acad Sci U S A. 2014 Sep 16;111(37):13535-40.

41. Jin J, Cheng J, Lee KW, Amreen B, McCabe KA, Pitcher C, Liebmann T, Greengard P, Flajolet M. Cholinergic neurons of the medial septum are crucial for sensorimotor gating. J Neurosci. 2019 Jun 26;39(26):5234-42.

42. Desikan S, Koser DE, Neitz A, Monyer H. Target selectivity of septal cholinergic neurons in the medial and lateral entorhinal cortex. Proc Natl Acad Sci U S A. 2018 Mar 13;115(11):E2644-e52.

43. Lehmann L, Lo A, Knox KM, Barker-Haliski M. Alzheimer's Disease and Epilepsy: A perspective on the opportunities for overlapping therapeutic innovation. Neurochem Res. 2021 Aug;46(8):1895-912.

44. Herreman A, Hartmann D, Annaert W, Saftig P, Craessaerts K, Serneels L, Umans L, Schrijvers V, Checler F, Vanderstichele H, Baekelandt V, Dressel R, Cupers P, Huylebroeck D, Zwijsen A, Van Leuven F, De Strooper B. Presenilin 2 deficiency causes a mild pulmonary phenotype and no changes in amyloid precursor protein processing but enhances the embryonic lethal phenotype of presenilin 1 deficiency. Proc Natl Acad Sci U S A. 1999 Oct 12;96(21):11872-7.

45. Salehi A, Delcroix JD, Belichenko PV, Zhan K, Wu C, Valletta JS, Takimoto-Kimura R, Kleschevnikov AM, Sambamurti K, Chung PP, Xia W, Villar A, Campbell WA, Kulnane LS, Nixon RA, Lamb BT, Epstein CJ, Stokin GB, Goldstein LS, Mobley WC. Increased APP expression in a mouse model of Down's syndrome disrupts NGF transport and causes cholinergic neuron degeneration. Neuron. 2006 Jul 6;51(1):29-42.

46. Lisgaras CP, Scharfman HE. Robust chronic convulsive seizures, high frequency oscillations, and human seizure onset patterns in an intrahippocampal kainic acid model in mice. Neurobiol Dis. 2022 Jan 25:105637.

47. Zhu H, Aryal DK, Olsen RH, Urban DJ, Swearingen A, Forbes S, Roth BL, Hochgeschwender U. Cre-dependent DREADD (Designer Receptors Exclusively Activated by Designer Drugs) mice. Genesis. 2016 Aug;54(8):439-46.

48. Roth BL. DREADDs for Neuroscientists. Neuron. 2016 2016/02/17/;89(4):683-94.

49. Smith KS, Bucci DJ, Luikart BW, Mahler SV. DREADDS: Use and application in behavioral neuroscience. Behav Neurosci. 2016 Apr;130(2):137-55.

50. Jendryka M, Palchaudhuri M, Ursu D, van der Veen B, Liss B, Kätzel D, Nissen W, Pekcec A. Pharmacokinetic and pharmacodynamic actions of clozapine-N-oxide, clozapine, and compound 21 in DREADD-based chemogenetics in mice. Sci Rep. 2019 Mar 14;9(1):4522.

51. Manvich DF, Webster KA, Foster SL, Farrell MS, Ritchie JC, Porter JH, Weinshenker D. The DREADD agonist clozapine N-oxide (CNO) is reverse-metabolized to clozapine and produces clozapine-like interoceptive stimulus effects in rats and mice. Sci Rep. 2018 Mar 1;8(1):3840.

52. Whissell PD, Tohyama S, Martin LJ. The Use of DREADDs to deconstruct behavior. Front Genet. 2016;7:70.

53. Lisgaras CP, Oliva A, McKenzie S, LaFrancois J, Siegelbaum SA, Scharman HE. Hippocampal area CA2 controls seizure dynamics, interictal EEG abnormalities and social comorbidity in mouse models of temporal lobe epilepsy. bioRxiv. 2023 Jan 18.

54. Navarrete M, Alvarado-Rojas C, Le Van Quyen M, Valderrama M. RIPPLELAB: A comprehensive application for the detection, analysis and classification of high frequency oscillations in electroencephalographic signals. PLoS One. 2016;11(6):e0158276.

55. Oliva A, Fernandez-Ruiz A, Buzsaki G, Berenyi A. Role of hippocampal CA2 region in triggering sharp-wave ripples. Neuron. 2016 Sep 21;91(6):1342-55.

56. Buzsáki G. Hippocampal sharp waves: their origin and significance. Brain Res. 1986 Nov 29;398(2):242-52.

57. Fernández-Ruiz A, Oliva A, Soula M, Rocha-Almeida F, Nagy GA, Martin-Vazquez G, Buzsáki G. Gamma rhythm communication between entorhinal cortex and dentate gyrus neuronal assemblies. Science. 2021 Apr 2;372(6537).

58. Staley KJ, Dudek FE. Interictal spikes and epileptogenesis. Epilepsy Currents. 2006 2006/11/01;6(6):199-202.

59. Avoli M, Biagini G, de Curtis M. Do interictal spikes sustain seizures and epileptogenesis? Epilepsy Curr. 2006 Nov-Dec;6(6):203-7.

60. Karoly PJ, Freestone DR, Boston R, Grayden DB, Himes D, Leyde K, Seneviratne U, Berkovic S, O'Brien T, Cook MJ. Interictal spikes and epileptic seizures: their relationship and underlying rhythmicity. Brain. 2016 Apr;139(Pt 4):1066-78.

61. Jayadev S, Leverenz JB, Steinbart E, Stahl J, Klunk W, Yu CE, Bird TD. Alzheimer's disease phenotypes and genotypes associated with mutations in presenilin 2. Brain. 2010 Apr;133(Pt 4):1143-54.

62. Zarea A, Charbonnier C, Rovelet-Lecrux A, Nicolas G, Rousseau S, Borden A, Pariente J, Le Ber I, Pasquier F, Formaglio M, Martinaud O, Rollin-Sillaire A, Sarazin M, Croisile B, Boutoleau-Bretonnière C, Ceccaldi M, Gabelle A, Chamard L, Blanc F, Sellal F, Paquet C, Campion D, Hannequin D, Wallon D. Seizures in dominantly inherited Alzheimer disease. Neurology. 2016 Aug 30;87(9):912-9.

63. Busche MA, Eichhoff G, Adelsberger H, Abramowski D, Wiederhold KH, Haass C, Staufenbiel M, Konnerth A, Garaschuk O. Clusters of hyperactive neurons near amyloid plaques in a mouse model of Alzheimer's disease. Science. 2008 Sep 19;321(5896):1686-9.

64. Hampel H, Mesulam MM, Cuello AC, Farlow MR, Giacobini E, Grossberg GT, Khachaturian AS, Vergallo A, Cavedo E, Snyder PJ, Khachaturian ZS. The cholinergic system in the pathophysiology and treatment of Alzheimer's disease. Brain. 2018 Jul 1;141(7):1917-33.

65. Bartus RT, Dean RL, 3rd, Beer B, Lippa AS. The cholinergic hypothesis of geriatric memory dysfunction. Science. 1982 Jul 30;217(4558):408-14.

66. DeKosky ST, Ikonomovic MD, Styren SD, Beckett L, Wisniewski S, Bennett DA, Cochran EJ, Kordower JH, Mufson EJ. Upregulation of choline acetyltransferase activity in hippocampus and frontal cortex of elderly subjects with mild cognitive impairment. Ann Neurol. 2002 Feb;51(2):145-55.

67. Hyman BT, Kromer LJ, Van Hoesen GW. Reinnervation of the hippocampal perforant pathway zone in Alzheimer's disease. Ann Neurol. 1987 Mar;21(3):259-67.

68. Mufson EJ, Counts SE, Perez SE, Ginsberg SD. Cholinergic system during the progression of Alzheimer's disease: therapeutic implications. Expert Rev Neurother. 2008 Nov;8(11):1703-18.

69. Trinh NH, Hoblyn J, Mohanty S, Yaffe K. Efficacy of cholinesterase inhibitors in the treatment of neuropsychiatric symptoms and functional impairment in Alzheimer disease: a meta-analysis. Jama. 2003 Jan 8;289(2):210-6.

70. Lahiri DK, Farlow MR. Review: cholinesterase inhibitors have a modest effect on neuropsychiatric and functional outcomes in Alzheimer's disease. Evid Based Ment Health. 2003 Aug;6(3):94.

71. Corbett BF, You JC, Zhang X, Pyfer MS, Tosi U, Iascone DM, Petrof I, Hazra A, Fu CH, Stephens GS, Ashok AA, Aschmies S, Zhao L, Nestler EJ, Chin J. ΔFosB regulates gene expression and cognitive dysfunction in a mouse model of Alzheimer's disease. Cell Rep. 2017 Jul 11;20(2):344-55.

72. Palop JJ, Jones B, Kekonius L, Chin J, Yu GQ, Raber J, Masliah E, Mucke L. Neuronal depletion of calcium-dependent proteins in the dentate gyrus is tightly linked to Alzheimer's disease-related cognitive deficits. Proc Natl Acad Sci U S A. 2003 Aug 5;100(16):9572-7.

73. Alcantara-Gonzalez D, Chartampila E, Criscuolo C, Scharfman HE. Early changes in synaptic and intrinsic properties of dentate gyrus granule cells in a mouse model of Alzheimer's disease neuropathology and atypical effects of the cholinergic antagonist atropine. Neurobiol Dis. 2021 May;152:105274.

74. Ulbert I, Heit G, Madsen J, Karmos G, Halgren E. Laminar analysis of human neocortical interictal spike generation and propagation: current source density and multiunit analysis in vivo. Epilepsia. 2004;45 Suppl 4:48-56.

75. Guth TA, Kunz L, Brandt A, Dümpelmann M, Klotz KA, Reinacher PC, Schulze-Bonhage A, Jacobs J, Schönberger J. Interictal spikes with and without high-frequency oscillation have different single-neuron correlates. Brain. 2021 Nov 29;144(10):3078-88.

76. Ohm TG. The dentate gyrus in Alzheimer's disease. In: Scharfman HE, editor. Progress in Brain Research: Elsevier; 2007. p. 723-40.

77. Ehrenberg AJ, Kelberman MA, Liu KY, Dahl MJ, Weinshenker D, Falgàs N, Dutt S, Mather M, Ludwig M, Betts MJ, Winer JR, Teipel S, Weigand AJ, Eschenko O, Hämmerer D, Leiman M, Counts SE, Shine JM, Robertson IH, Levey AI, Lancini E, Son G, Schneider C, Egroo MV, Liguori C, Wang Q, Vazey EM, Rodriguez-Porcel F, Haag L, Bondi MW, Vanneste S, Freeze WM, Yi Y-J, Maldinov M, Gatchel J, Satpati A, Babiloni C, Kremen WS, Howard R, Jacobs HIL, Grinberg LT. Priorities for research on neuromodulatory subcortical systems in Alzheimer's disease: position paper from the NSS PIA of ISTAART. Alzheimer's & Dementia.